Journal of Oceanography, Vol. 61, pp. 399 to 413, 2005

Drag Coefficient, Dynamic Roughness and Reference Wind Speed

Paul A. Hwang*

Oceanography Division, Naval Research Laboratory, Stennis Space Center, MS 39529-5004, U.S.A.

(Received 15 May 2004; in revised form 23 July 2004; accepted 26 July 2004)

Surface waves are the roughness element of the ocean surface. The parameterization of the drag coefficient of the ocean surface is simplified by referencing to wind speed at an elevation proportional to the characteristic wavelength. The dynamic roughness is analytically related to the drag coefficient. Under the assumption of fetch limited wave growth condition, various empirical functions of the dynamic roughness can be converted to equivalent expressions for comparison. For datasets covering a wide range of the dimensionless frequency (inverse wave age), it is important to account for the variable rate of wave development at different wave ages. As a result, the dependence of the Charnock parameter on wave age is nonmonotonic. Finally, the analysis presented here suggests that the significant wave steepness is a sensitive property of the ocean surface and a single variable normalization of the dynamic roughness using a wavelength or wave height parameter actually produces more robust functions than bi-variable normalizations using wave height and wave slope.

Keywords:
· Drag coefficient,
· dynamic roughness,
· wavelength,
· wave age,
· dimensionless frequency.

1. Introduction

Within the framework of the logarithmic wind profile, the drag coefficient, C_D, and dynamic roughness, z_0, are correlated deterministically. The analytical equation relating these two parameters can be readily derived. Analyses of field data on these two quantities, however, have produced many confusing or conflicting results. For example, the drag coefficient, a dimensionless parameter, is frequently expressed as a linear or nonlinear function of wind speed, U, a dimensional parameter. From dimensional considerations, such expressions are clearly inaccurate unless the system has a constant reference velocity, which is certainly not the case for air-sea interaction problems involving surface waves. The expression of $C_D(U)$ is apparently stipulated by operational needs and practical considerations. The adaptation of such functional form masks the influence of wave development and sea state factors, and eventually introduces errors into the end results of the analyses on air-sea interaction processes.

Another serious issue in the analysis of C_D and z_0 is the reference wind speed, which is typically taken as U_{10}, the neutral wind speed at 10 m elevation. Fixing the height for wind speed reference at 10 m is also obviously derived from operational or practical considerations rather than the dynamical significance of the 10-m elevation in the marine boundary layer. Because the influence of surface waves decays exponentially with the wavelength serving as the vertical length scale (e.g., Miles, 1957; Phillips, 1977), the dynamically meaningful reference elevation should be the characteristic wavelength, λ_p (e.g., Kitaigorodskii, 1973; Stewart, 1974; Donelan, 1990; Makin and Kudryavtsev, 1999, 2002; Makin, 2003; Hwang, 2004, 2005). In this paper, the reference wind speed, $U_{\lambda/2}$, is taken at the elevation of one-half wavelength. The drag coefficient, dimensionless roughness (e.g., k_pz_0, where z_0 is the dynamic roughness and $k_p = 2\pi/\lambda_p$ the characteristic wavenumber, or the Charnock parameter (1955) $z_{0*} = gz_0/u_*^2$, where g is the gravitational acceleration and u_* the friction velocity) and dimensionless frequency, ω_* ($=U_{\lambda/2}/c_p$, the inverse wave age for deep water condition, c_p is the phase velocity for the spectral peak component), are uniquely defined (Section 2). A comparison of C_{10} and $C_{\lambda/2}$, the drag coefficient referenced to U_{10} and $U_{\lambda/2}$, respectively, is carried out. The systematic influence of surface wavelength on C_{10} can be detected in field measurements taken under fetch limited wave conditions (e.g., Donelan, 1979; Merzi and Graf, 1985; Anctil and Donelan, 1996; Janssen, 1997). The wavelength influence is mostly removed when $C_{\lambda/2}$ is processed instead of C_{10}. The detail is given by Hwang (2004, 2005). A brief summary is presented in Section 3. The results on the analysis of the drag coefficient indi-

* E-mail address: paul.hwang@nrlssc.navy.mil

cate that $R_C = C_{10}/C_{\lambda/2}$ increases with ω_* when $\lambda_p < 20$ m and decreases with ω_* when $\lambda_p > 20$ m. The controversy of the roughness dependence on wave age (e.g., Donelan, 1990; Toba *et al.*, 1990; Donelan *et al.*, 1993; Jones and Toba, 2001) can be attributed partially to this behavior, and will be discussed in more detail in Section 4. It is noted that Oost *et al.* (2002) also demonstrate an excellent correlation between u_* and $U_{\lambda/2}$ or U_λ for data under neutral stratification and wind sea dominant conditions, with a correlation coefficient of 0.964. Empirical functions of C_λ were given.

Several different expressions of the dimensionless roughness have been proposed (e.g., Donelan, 1990; Toba *et al.*, 1990; Smith *et al.*, 1992; Donelan *et al.*, 1993; Taylor and Yelland, 2001). For a wave system under active wind forcing, the robust fetch growth functions can be applied to compare these different expressions. The results are very sensitive to the exponent of the power law relating the dimensionless wave energy and wave frequency, $e_*(\omega_*)$. Hereafter the exponent is referred to as the development rate. Because the variation of the development rate is substantial at different ω_* ranges of the field data (Appendix A), opposite trends in the dependence of z_{0*} on ω_* in different ω_* ranges can occur. The detail is described in Section 4. Additional discussions on the scaling issues and dimensional analysis are given in Section 5. Finally, a summary is presented in Section 6.

2. Reference Wind Speed for the Drag Coefficient and Dynamic Roughness

Based on the logarithmic wind speed profile for neutral stratification, the vertical distribution of the wind speed is given by

$$U_z = \frac{u_*}{\kappa}\ln\frac{z}{z_0} = \frac{u_*}{\kappa}\ln\frac{k_p z}{k_p z_0}, \tag{1}$$

where κ is the von Kármán constant and z is the vertical elevation measured from the mean water surface. In the second part of (1), the wavenumber is introduced to emphasize that the relevant vertical length scale is the surface wavelength. Referenced to $U_{\lambda/2}$, the drag coefficient $C_{\lambda/2} = u_*^2/U_{\lambda/2}^2$ can be derived from (1)

$$C_{\lambda/2} = \left[\frac{1}{\kappa}\ln\left(\frac{\pi}{k_p z_0}\right)\right]^{-2} = \left[\frac{1}{\kappa}\ln\left(\frac{\pi}{z_{0*}\omega_{**}^2}\right)\right]^{-2}, \tag{2}$$

where $\omega_{**} = \omega_p u_*/g$ is a dimensionless frequency. In this and the next sections, the deep water wave condition is assumed for simplicity. Effects of finite water depth will be introduced in Section 4. Evidence of logarithmic profile holds to height of $\lambda/2$ is frequently observed in laboratory measurements. In the field, the dataset of Merzi and Graf (1985) is an excellent example. They conducted wind stress measurements in Lake Geneva. The measurement station is on the northern part of the lake. The records selected for analysis are based on steady southwesterly events and well-behaved wind profiles (60 cases), for the fetch-growth wave conditions. The friction velocity is derived from the profile method applied to measurements by five anemometers mounted at 12.12, 7.27, 4.27, 2.42 and 1.80 m above the mean water surface. The maximum and minimum wavelengths in this dataset are 19.0 and 8.6 m, so their measurements do reach to the elevation of $\lambda/2$ with well-behaved wind profiles.

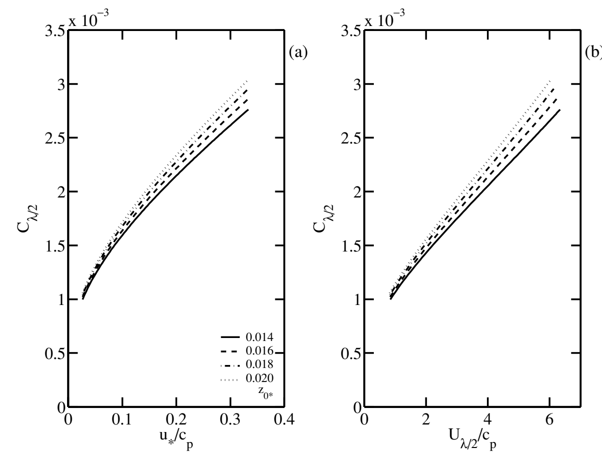

Fig. 1. Dimensionless expressions of the drag coefficient, (a) $C_{\lambda/2}(\omega_*)$, (b) $C_{\lambda/2}(\omega_{**})$, with z_{0*} as a parameter.

In deep water $\omega_{**} = \omega_p u_*/g = u_*/c_p$ is a measure of the inverse wave age. As mentioned earlier, the dimensionless frequency can also be defined using $U_{\lambda/2}$ and g, that is, $\omega_* = \omega_p U_{\lambda/2}/g = U_{\lambda/2}/c_p$. The two expressions of the dimensionless frequency are related by $\omega_{**}^2 = \omega_*^2 C_{\lambda/2}$, thus, (2) can also be expressed as

$$C_{\lambda/2} = \left[\frac{1}{\kappa}\ln\left(\frac{\pi}{z_{0*}C_{\lambda/2}\omega_*^2}\right)\right]^{-2}. \tag{3}$$

Depending on the functional form of the dimensionless roughness expressed as the Charnock parameter, z_{0*}, either (2) or (3) may be more convenient to use for computation. For example, if z_{0*} is assumed constant or a function of ω_{**}, (2) is obviously a better choice. $C_{\lambda/2}(\omega_{**})$ can be easily computed with ω_{**} as the only independent variable. To present $C_{\lambda/2}(\omega_*)$, $\omega_* = \omega_{**}C_{\lambda/2}^{0.5}$ can be calculated once $C_{\lambda/2}(\omega_{**})$ is evaluated. In comparison, to obtain $C_{\lambda/2}(\omega_*)$ using (3) would require nonlinear iterations.

On the other hand, if the dynamic roughness is expressed as $z_0/\eta_{rms} = f(k_p\eta_{rms}, \omega_*)$, where η_{rms} is the root mean square (rms) surface elevation (e.g., Donelan, 1990; Smith *et al.*, 1992; Donelan *et al.*, 1993; Anctil and Donelan, 1996; Taylor and Yelland, 2001), the functions transform to $z_{0*}C_{\lambda/2} = f(\omega_*)$, and (3) is easier for application. The detail is described further in Section 4.

For the purpose of illustration, the functional dependence of $C_{\lambda/2}(\omega_{**})$ and $C_{\lambda/2}(\omega_*)$ are presented in Figs. 1(a) and (b), respectively for a range of z_{0*} between 0.014 and 0.020. The magnitude of $C_{\lambda/2}$ varies from about 0.001 to 0.003, which is within the commonly observed range. The increasing trend of $C_{\lambda/2}$ with wind speed (for a constant c_p) is in agreement with various linear or nonlinear expressions of $C_{10}(U_{10})$, and (2) and (3) are dimensionally consistent.

Published papers rarely report $C_{\lambda/2}$ and $U_{\lambda/2}$. Instead, the experimental results are usually presented as C_{10} and U_{10}, the drag coefficient and reference wind speed at 10 m elevation. Although quantities referenced to a fixed elevation are more convenient to use and may even be necessary from an operational point of view, such utilization does create considerable problems for subsequent investigations of the air-sea interaction processes, as will be described further in the following sections. Hwang (2005) presents parameterization functions of $C_{\lambda/2}$ on ω_pU_{10}/g and U_{10}/c_p for practical applications. The result illustrates that the wind stress computed from U_{10} using $C_{\lambda/2}$ parameterizations is more accurate than the wind stress calculated with various C_{10} parameterization functions. A brief summary of that study is presented in Appendix B.

3. Drag Coefficient

Using the reference wind speed at 10 m elevation, the drag coefficient becomes

$$C_{10} = \left[\frac{1}{\kappa}\ln\left(\frac{k_p 10}{k_p z_0}\right)\right]^{-2} = \left[\frac{1}{\kappa}\ln\left(\frac{k_p 10}{z_{0*}\omega_{**}^{2}}\right)\right]^{-2}. \quad (4)$$

The effect of using a fixed-elevation reference wind speed on the drag coefficient can be quantified by the ratio

$$R_C = \frac{C_{10}}{C_{\lambda/2}} = \left[\frac{\ln\left(\frac{\pi}{k_p z_0}\right)}{\ln\left(\frac{10k_p}{k_p z_0}\right)}\right]^2 = \left[\frac{\ln\left(\frac{\pi}{z_{0*}\omega_{**}^{2}}\right)}{\ln\left(\frac{10k_p}{z_{0*}\omega_{**}^{2}}\right)}\right]^2. \quad (5)$$

Inspecting (5), it is quite obvious that R_C varies with surface wavelength, $\lambda_p = 2\pi/k_p$, in addition to the dimensionless parameter k_pz_0 $(=z_{0*}\omega_{**}^2 = z_{0*}\omega_*^2C_{\lambda/2})$. In particular, the variation of $R_C(\omega_{**})$ or $R_C(\omega_*)$ differs in the two wavelength regions separated by $\lambda_p = 20$ m, under which condition $z = 10$ m $= \lambda_p/2$ is the proper reference level: R_C increases with ω_* for $\lambda_p < 20$ m, and the trend reverses for $\lambda_p > 20$ m. The impact is especially large at young sea state and is still substantial at more mature wave conditions. The drag coefficient presented in Fig. 1 is recast in C_{10} and plotted in Fig. 2 for three wavelengths $\lambda_p = 10$, 20 and 40 m to illustrate the additional k_p influence on the C_{10} expression (4). The results are presented first in dimensionless forms $C_{10}(u_*/c_p)$ and $C_{10}(U_{10}/c_p)$ in Figs. 2(a) and (b), respectively. Comparing Fig. 2 with Fig. 1 it is readily seen that a significant increase in data scatter can be expected when the drag coefficient is represented by C_{10}. The situation is more complicated when the dimensionally inconsistent form $C_{10}(U_{10})$ is used (Fig. 2(c)). The increasing trend of $C_{10}(U_{10}/c_p)$ with increasing λ_p for a given z_{0*} seems to disappear when viewed as $C_{10}(U_{10})$. The apparent disappearance of the wavelength factor in $C_{10}(U_{10})$ as shown in Fig. 2(c) is deceptive as it is the result of the assumption of constant z_{0*} used in these illustrative examples. Applying the dispersion relation, (4) can be rewritten as

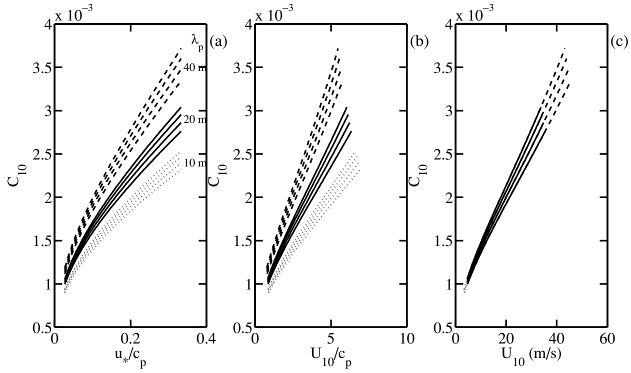

Fig. 2. Drag coefficient presented as (a) $C_{10}(u_*/c_p)$, (b) $C_{10}(U_{10}/c_p)$, and (c) $C_{10}(U_{10})$. The computations are based on the same conditions presented in Fig. 1.

$$C_{10} = \left[\frac{1}{\kappa}\ln\left(\frac{g10}{z_{0*}u_*^{2}}\right)\right]^{-2} = \left[\frac{1}{\kappa}\ln\left(\frac{g10}{z_{0*}C_{10}U_{10}^{2}}\right)\right]^{-2}. \quad (4a)$$

If z_{0*} is not constant but varies as a function of u_*/c_p or U_{10}/c_p (see Section 4), say $z_{0*} = A_1(U_{10}/c_p)^{a_1}$, the product $z_{0*}U_{10}^2$ in (4a) becomes $A_1U_{10}^{2+a_1}c_p^{-a_1}$. The additional wavelength effect through c_p becomes evident. In comparison, with (2) or (3), when z_{0*} is expressed as a

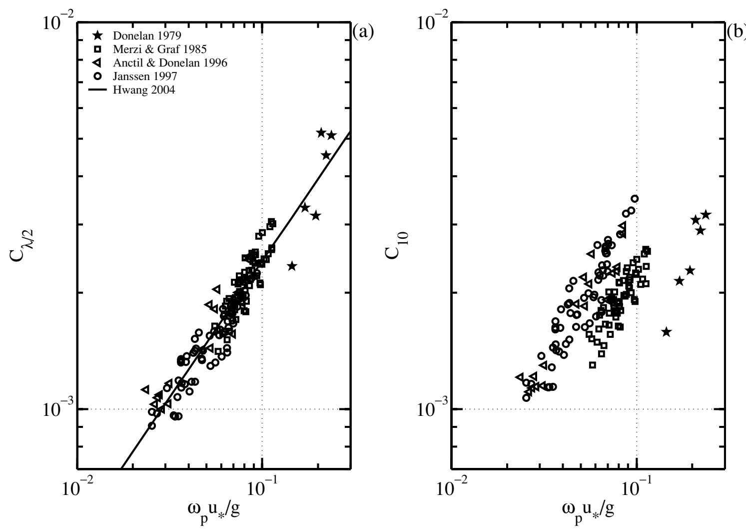

Fig. 3. Field measurements of wind stress in fetch limited conditions presented as (a) $C_{\lambda/2}(\omega_{**})$, and (b) $C_{10}(\omega_{**})$. The range of wavelengths is [3.3, 5.7], [8.6, 19.0], [28.6, 75.8] and [56.4, 101.6] for Donelan (1979), Merzi and Graf (1985), Anctil and Donelan (1996) and Janssen (1997), respectively.

function of ω_* or ω_{**}, a unique correlation of $C_{\lambda/2}(\omega_*)$ or $C_{\lambda/2}(\omega_{**})$ is established. It is also clear from (4a) that the reference velocity scale in the expression of $C_{10}(U_{10})$ is the constant $(gz_{ref})^{0.5}$ with z_{ref} = 10 m. As noted previously, the significance of this constant reference velocity scale in the marine boundary layer dynamics is rather vague.

Hwang (2004) applies the above analysis of wavelength parameterization of the ocean surface drag coefficient to measurements from four field experiments conducted under fetch limited wave growth conditions (Donelan, 1979; Merzi and Graf, 1985; Anctil and Donelan, 1996; and Janssen, 1997). The results show that a strong similarity relation exists when the drag coefficient is expressed as $C_{\lambda/2}(\omega_{**})$. The correlation coefficient, Q, of the scatter plot is 0.95 and the relative rms difference, S, is 0.017 (Fig. 3(a)). For comparison, the corresponding statistics for $C_{10}(\omega_{**})$ are 0.74 and 0.028 (Fig. 3(b)). The range of wavelengths is [3.3, 5.7], [8.6, 19.0], [28.6, 75.8] and [56.4, 101.6] for Donelan (1979), Merzi and Graf (1985), Anctil and Donelan (1996) and Janssen (1997), respectively. Stratification with wavelength in the C_{10} representation of the ocean surface drag coefficient is quite apparent (Fig. 3(b)). More discussions on the wavelength scaling of the drag coefficient and validation with field data can be found in Hwang (2004, 2005).

4. Dynamic Roughness

4.1 Typical parameterization functions

As mentioned earlier, recent investigations of the dynamic roughness have concluded that the Charnock parameter is not a constant and z_0 parameterization needs to incorporate wave parameters. Kitaigorodskii and Volkov (1965) consider the wind-wave momentum transfer in the frame of reference moving with the phase speed of surface waves. The logarithmic wind profile then leads to the following dimensionless expression of the dynamic roughness

$$\frac{z_0}{\eta_{rms}} \sim \exp\left(-\kappa \frac{c_p}{u_*}\right). \tag{6}$$

A simplified form is given by Kitaigorodskii (1973)

$$\frac{z_0}{\eta_{rms}} = 0.3 \exp\left(-\kappa \frac{c_p}{u_*}\right). \tag{7}$$

In the three decades following the introduction of (7), many experiments were conducted. The results generally confirm the effects of surface waves on the drag coefficient and dynamic roughness, but the wave related signal in the measured stress is not sufficiently clear for researchers "*to agree on its form, much less its size*" as observed by Donelan (1990), who provides an excellent review of the state of development. He further concludes that "*A consistent parameterization of the roughness of sea surface in terms of the wave field will only be possible when we are able to strengthen the wave related signal (by widening the range of wave development in our observations) and to suppress the noise in our measurements. Given* *the requirement for stationarity and horizontal homogeneity in the wind, fetch-limited studies are probably the only way to achieve the former goal.*" With this in mind, he assembled a dataset of field measurements covering a wide range of the wave age parameter ($U_{10}/c_p \cong 0.8$–5) and carefully screened for fetch-limited requirements. The data scatter is considerable but the result show a clear regression trend of

$$\frac{z_0}{\eta_{rms}} = A_0\left(\frac{v}{c_p}\right)^{a_0}, \tag{8}$$

where the velocity scale v can be U_{10}, $U_{\lambda/2}$ or u_*. To further widen the wave age coverage, laboratory results are added but the two data populations show clear differences. The coefficients and exponents [A_0, a_0] for the field dataset are [5.53×10^{-4}, 2.66], [3.70×10^{-4}, 3.38] and [1.84, 2.53], respectively for U_{10}, $U_{\lambda/2}$ and u_* serving as the scaling velocity. Smith *et al*. (1992) report a similar correlation but with a larger exponent for the fitting parameters [5.32×10^{-4}, 3.53] for their data in the range of U_{10}/c_p between 2 and 4 (the plot shown in their figure 12 is off by a factor of 2). Donelan *et al*. (1993) comments that the curve

$$\frac{z_0}{\eta_{rms}} = 5.5\times10^{-4}\left(\frac{U_{10}}{c_p}\right)^{2.7} = A_{zU}\omega_*^{a_{zU}} \tag{9}$$

fits the combined datasets equally well as the steeper fitting function suggested by Smith *et al*. (1992).

Anctil and Donelan (1996) and Taylor and Yelland (2001) present analyses showing that including the sea surface slope parameter can reduce fitting error. The root mean square slope is used in the work by Anctil and Donelan (1996). Taylor and Yelland (2001) use the ratio of significant wave height and peak wavelength as a characteristic surface steepness. Using the notations of this paper, Taylor and Yelland's (2001) equation can be expressed as

$$\frac{z_0}{\eta_{rms}} = 629.07 s_*^{2.25} = A_{zs} s_*^{a_{zs}}, \tag{10}$$

where $s_* = k_p^2 \eta_{rms}^2$.

Toba *et al*. (1990) use u_* and ω_p instead of wave height or wave slope to normalize the dynamic roughness, and suggest that

$$\frac{z_0 \omega_p}{u_*} = \gamma, \quad \gamma = 0.025. \tag{11}$$

4.2 Conversion to equivalent expressions

As described in Section 2, the dynamic roughness and wind stress or drag coefficient are uniquely connected when wind speed is referenced at an elevation proportional to the surface wavelength (2). The dimensionless form of dynamic roughness is explicitly $k_p z_0$, which can appear in several difference forms through the use of the dispersion relation

$$\omega_p^2 = g k_p \tanh k_p h, \tag{12}$$

where h is water depth:

$$\begin{aligned} k_p z_0 &= z_{0*}\left(\frac{u_*}{c_p}\right)^2 \tanh k_p h = z_{0*}\omega_{**}^2 \frac{1}{\tanh k_p h} \\ &= z_{0*}\omega_*^2 C_{\lambda/2} \frac{1}{\tanh k_p h}. \end{aligned} \tag{13}$$

The functional dependence of z_0 on wind and wave parameters is not yet fully established, as reflected by the large number of parameterization functions reported in the literature. The functions outlined in Subsection 4.1 represent but a small sample. Here the behavior of z_{0*} is investigated with three generic functions that explicitly incorporate the surface wave parameters. The generic functions are converted to equivalent expressions for comparison assuming fetch limited wave conditions. The dimensionless wave frequency and wave energy are expressed as $\omega_{**} = \omega_p u_*/g \equiv (u_*/c_p)\tanh kh$ and $e_{**} = \eta_{rms}^2 g^2/u_*^4$. The wave steepness can be expressed in terms of ω_{**} and e_{**} by $s_* = k_p^2 \eta_{rms}^2 \equiv e_{**}\omega_{**}^4/\tanh^2 kh$. For clarity, only the results with (u_*/c_p) scaling in (13) are given here.

a. $z_0/\eta_{rms} \sim u_*/c_p$ *(e.g., Donelan, 1990; Smith et al., 1992)*

Expressing the dimensionless roughness as

$$\frac{z_0}{\eta_{rms}} = A_{zu}\left(\frac{u_*}{c_p}\right)^{a_{zu}}, \tag{14}$$

(13) can be written as

$$z_{0*} = A_{zu} e_{**}^{0.5}\left(\frac{u_*}{c_p}\right)^{a_{zu}}. \tag{15}$$

Using the fetch law (Appendix A)

$$e_{**} = A_{eu}\left(\frac{u_*}{c_p}\right)^{a_{eu}}, \tag{16}$$

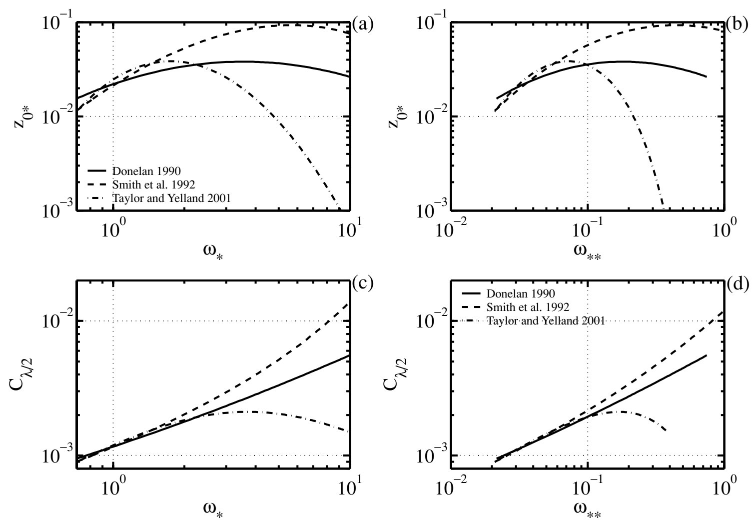

Fig. 4. Computed results showing the wave-age dependence of dynamic roughness and drag coefficient based on several different parameterization functions (see legend) recast into same functional form through the application of fetch-limited growth laws: (a) $z_{0*}(\omega_*)$, (b) $z_{0*}(\omega_{**})$, (c) $C_{\lambda/2}(\omega_*)$, and (d) $C_{\lambda/2}(\omega_{**})$.

then whether z_{0*} increases or decreases with u_*/c_p depends on whether $(0.5a_{eu} + a_{zu})$ is greater than or less than zero. One common practice in the analysis of dynamic roughness data is to assume that $e_{**}(u_*/c_p)$ can be expressed as a simple power-law function, that is, a_{eu} is constant. When the range of u_*/c_p is large, this assumption is inaccurate. Field measurements show that a_{eu} is negative and the magnitude increases with u_*/c_p (e.g., Donelan *et al*., 1985; Young, 1999; Hwang and Wang, 2004; and the results summarized in Appendix A).

b. $z_0/\eta_{rms} \sim k_p\eta_{rms}$ (e.g., Anctil and Donelan, 1996; Taylor and Yelland, 2001)

This relation can be written as

$$\frac{z_{0*}}{\eta_{rms}} = A_{zs} s_*^{\,a_{zs}}. \tag{17}$$

With the substitution of $s_* = k_p^2\eta_{rms}^2 = e_{**}\omega_{**}^4/\tanh^2 kh = e_{**}(u_*/c_p)^4\tanh^2 kh$, (13) can be written as

$$z_{0*} = A_{zs} e_{**}^{0.5+a_{zs}} \left(\frac{u_*}{c_p}\right)^{4a_{zs}} \tanh^{2a_{zs}} kh. \tag{18}$$

Substituting (16) to (18), the exponent of $z_{0*}(u_*/c_p)$ is $4a_{zs} + (0.5 + a_{zs})a_{eu}$ and can be either positive or negative.

c. $z_0\omega_p/u_* \sim$ constant (Toba et al., 1990)

With the substitution of

$$\frac{z_0\omega_p}{u_*} = \gamma = \text{a constant}, \tag{19}$$

(19) becomes

$$z_{0*} = \gamma\left(\frac{u_*}{c_p}\right)^{-1}\frac{1}{\tanh kh} = \gamma\omega_{**}^{\,-1}. \tag{20}$$

For this functional form, the roughness z_{0*} is expected to decrease with increasing u_*/c_p.

As shown above, various expressions of the dimensionless roughness can be recast into $z_{0*}(\omega_*)$ with the help of fetch-growth functions. Ideally, the fetch functions should be scaled with $U_{\lambda/2}$ or u_*, e.g.,

$$e_* = A_{ex}x_*^{\,a_{ex}}, \quad \omega_* = A_{\omega x}x_*^{\,a_{\omega x}}, \quad e_* = A_{e\omega}\omega_*^{\,a_{e\omega}}, \tag{21a--c}$$

where $e_* = \eta_{rms}^2 g^2/U_{\lambda/2}^4$, $x_* = xg/U_{\lambda/2}^2$ and $\omega_* = \omega_p U_{\lambda/2}/g$, (9) to (11) become

$$z_{0*}C_{\lambda/2} = A_{zU}A_{e\omega}^{0.5}\omega_*^{\,a_{zU}+0.5a_{e\omega}}, \tag{22}$$

$$z_{0*}C_{\lambda/2} = A_{zs}A_{e\omega}^{(a_{zs}+0.5)}\omega_*^{\,4a_{zs}+(a_{zs}+0.5)a_{e\omega}}, \tag{23}$$

$$z_{0*}C_{\lambda/2}^{0.5} = \gamma\omega_*^{-1}. \tag{24}$$

Currently, fetch growth data report U_{10} as the reference wind speed. Conversion to u_* relies on the application of a $C_{10}(U_{10})$ formula. As already discussed in Section 2, wave influences cannot be retrieved without explicit incorporation of wavelength into the C_{10} formula.

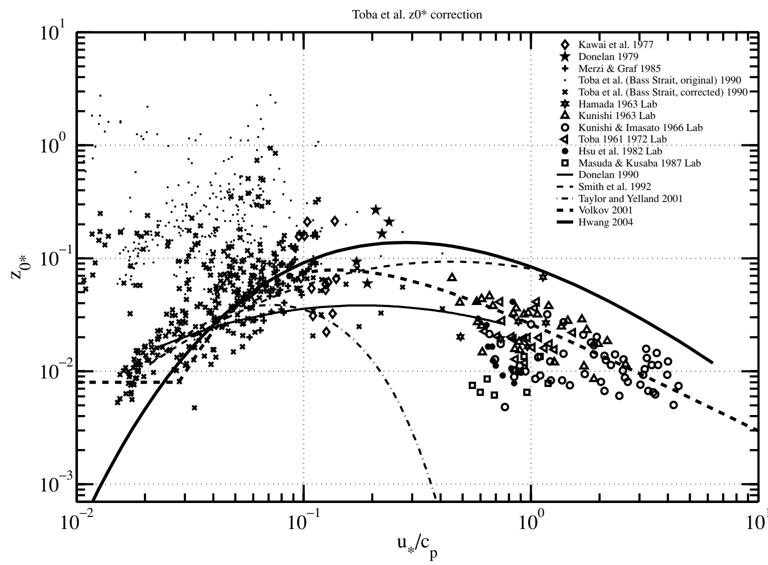

Fig. 5. Wave age dependence of the dynamic roughness and comparison of computations with measurements. Field data are from Toba *et al*. (1990). Curves are (22)–(27). Both original and corrected versions of the Bass Strait data are shown.

In the absence of ideal fetch growth laws, the ones scaled with U_{10} (Appendix A) are employed in the following discussions. For (22), the observed exponent a_{zU} ranges from 2.66 to 3.53, and the exponent $a_{e\omega}$ ranges from –2.7 at $\omega_* \approx 0.8$ to –4.1 at $\omega_* \approx 6$ (Fig. A2), so $z_{0*}C_{\lambda/2} \sim \omega_*^{(0.61-2.28)}$. With the observed exponent of $C_{\lambda/2}(\omega_*)$ about 1 (estimated from the fetch limited field data reported by Donelan, 1979; Merzi and Graf, 1985; Anctil and Donelan, 1996; Janssen, 1997), the exponent in the power law of $z_{0*}(\omega_*)$ can indeed become negative at the high ω_* range. Similarly, for (23) using $a_{zs} = 2.25$ (Taylor and Yelland, 2001), the exponent of $z_{0*}C_{\lambda/2}(\omega_*)$ is $9 + 2.75a_{e\omega}$, and ranges from 2.28 at $\omega_* \approx 0.8$ to –5.43 at $\omega_* \approx 6$. Figures 4(a) and (b) shows the numerical computations of the dynamic roughness using wave-age-dependent $A_{e\omega}$ and $a_{e\omega}$ (Appendix A) and two sets of A_{zU} and a_{zU} [5.53×10^{-4}, 2.66] and [5.32×10^{-4}, 3.53], representing (22); and A_{zs} and a_{zs} [630.51, 2.25] representing (23). The corresponding drag coefficient computed from the dimensionless roughness using (2) is shown in Figs. 4(c) and (d) as a function of ω_* and ω_{**}, respectively. For the range $\omega_* < 2$ or $\omega_{**} < 0.1$, the calculated results from these three equations are quite similar. As ω_* or ω_{**} increases the three curves diverge. In particular the steepness dependent formulation proposed by Taylor and Yelland (2001) produces a decreasing trend of the drag coefficient in high ω_* or ω_{**} conditions.

4.3 Comparison with data

Experimental data collected over a wide ω_* range show a similar nonmonotonic trend of $z_{0*}(\omega_*)$ as displayed in Fig. 4. This subsection presents comparisons with several datasets. In addition to the three formulas summarized in Subsection 4.2, two additional parameterization functions are also included for comparison. The first one is given by Volkov (2001), derived from relating z_0 with a wave-age dependent spectral model,

$$z_{0*} = \begin{cases} 0.03\left(\dfrac{c_p}{u_*}\right)\exp\left\{-0.14\left(\dfrac{c_p}{u_*}\right)\right\}, & 0.35 < \dfrac{c_p}{u_*} < 35 \\ 0.008, & \dfrac{c_p}{u_*} > 35. \end{cases} \tag{25}$$

The second is given by Hwang (2004), obtained from least square fitting of field data obtained under fetch limited wave conditions (Fig. 3(a))

$$C_{\lambda/2} = 0.0122\omega_{**}^{0.704}, \tag{26}$$

which can be converted to $z_{0*}(\omega_{**})$ through (2) for the deep water condition,

$$\begin{aligned} z_{0*} &= \pi\omega_{**}^{-2}\exp\left[-\kappa C_{\lambda/2}^{-0.5}\right] \\ &= \pi\omega_{**}^{-2}\exp\left[-\kappa\left(0.0122\omega_{**}^{0.704}\right)^{-0.5}\right]. \end{aligned} \tag{27}$$

Figure 5 compares the calculated results with the data reported by Toba *et al*. (1990). As mentioned earlier, the

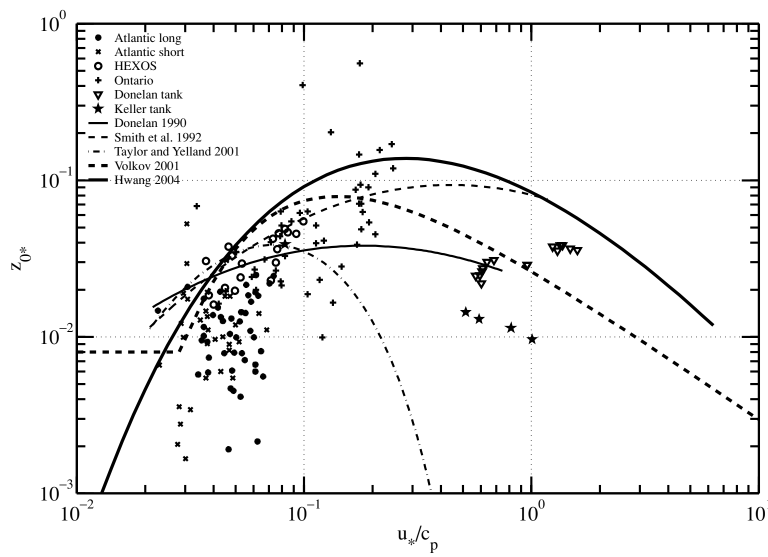

Fig. 6. Same as Fig. 5 but for the data assembled by Donelan *et al.* (1993).

Bass Strait data reported by Toba *et al.* (1990) do not have direct wind stress measurement and u_* is computed from a wind-dependent empirical formula connecting U_{10}, wave period and wave height. From the analysis presented in Section 2, evaluation of u_* using U_{10} is quite tricky. In particular, if C_{10} is used in place of $C_{\lambda/2}$ in (27), which is equivalent to discounting the wavelength factor when the drag coefficient is referenced to U_{10}, the error in z_{0*} estimation can be quantified by the ratio

$$R_z = \frac{z_{0*10}}{z_{0*}} = \frac{\exp\left(-\kappa C_{10}{}^{-0.5}\right)}{\exp\left(-\kappa C_{\lambda/2}^{-0.5}\right)} = \frac{\pi}{10k} = \frac{\lambda}{20}, \qquad (28)$$

where subscript 10 for z_{0*} emphasizes that the dimensionless roughness is calculated from using C_{10} in place of $C_{\lambda/2}$ in (27). The roughness calculated using C_{10} may represent the true dynamic roughness when $\lambda_p = 20$ m. For other wavelengths R_z is linearly proportional to the wavelength. This may explain the much larger magnitude of z_{0*10} (calculated from U_{10}) of the Bass Strait data in comparison with other datasets with direct wind stress measurements. Using wavelengths calculated from the wave periods recovered from figures 12 and 13 of Toba *et al.* (1990), the correction factor (28) is applied to the Bass Strait data. As shown in Fig. 5, the magnitudes of the corrected Bass Strait data lie in a much more reasonable range. The overall trend of the calculations based on (22)–(27) is in agreement with the large collection of data.

Figure 6 shows the comparison with six datasets assembled by Donelan *et al.* (1993). The Atlantic data are distributed over a narrow u_*/c_p range and the magnitudes of the roughness spread over a very wide range. This suggests strong swell influence. The function derived from fetch limited data sets (26) and (27) serves as the upper bound of the data cloud in this collection. Given the large data scatter, the agreement between computations and measurements is judged to be reasonably good.

5. Discussions

5.1 Reference length scale

Hwang (2004) emphasizes that if the reference wind speed is taken at an elevation proportional to the characteristic wavelength, $k_p z_0$ becomes the natural expression of the dimensionless roughness (2). Figures 7(a) and (b) present a comparison of the dimensionless roughness expressed as z_{0*} and $k_p z_0$ for the fetch limited data shown in Fig. 3. For $z_{0*}(\omega_{**})$, the statistics of correlation coefficient and normalized rms difference $(Q, S) = (0.80, 0.16)$, which are considerably worse than (0.95, 0.062) for $k_p z_0(\omega_{**})$. The dimensionless roughness expressed as z_0/H_s (Fig. 7(c)) also achieves very good correlation statistics, with $(Q, S) = (0.93, 0.076)$, only slightly worse than those of the $k_p z_0$ function. The almost equivalent performance of k_p and H_s serving as the vertical length scale for normalization is expected as a consequence of the similarity properties of wind-generated ocean wave spectrum for wind-sea dominant conditions. Although "sand roughness" equivalence is sometimes evoked to explain the proportionality between z_0 and H_s, it is noted that the ratio z_0/H_s expands several orders of magnitude (Fig. 7(c)), a range considerably larger than the observed ratio between the equivalent roughness and actual height of pro-

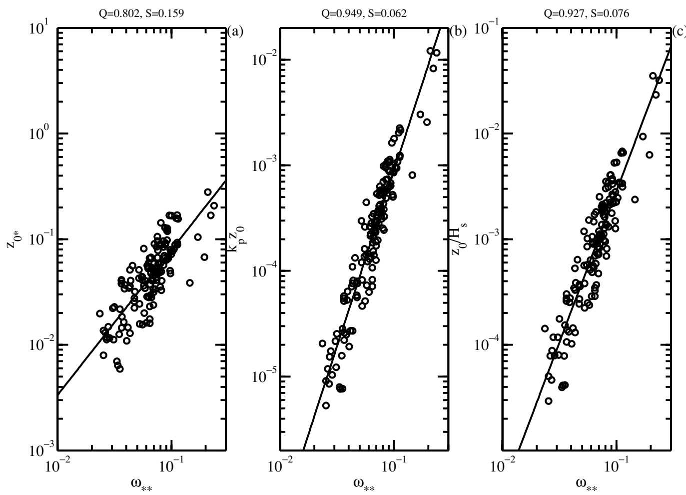

Fig. 7. Dimensionless roughness in terms of (a) z_{0*}, (b) $k_p z_0$, and (c) z_0/H_s, for fetch limited data shown in Fig. 3.

trusions in the measurement of fluid drag induced by regular roughness patterns (e.g., Schlichting, 1968). The difference suggests that for the ocean surface, drag components contributed by regular roughness geometry (surface waveform), such as skin friction and form drag, are only partial contributors to the total surface stress. Other dynamic processes, such as flow separation attributed to wave breaking, may be quite important (e.g., Banner and Melville, 1976; Kawai, 1982; Makin and Kudryavtsev, 1999, 2002; Makin, 2003). While wave height and wavelength are both major characteristics of surface waves, wavelength may play a more important role because the dynamic influences of waves typically decay exponentially with wavelength serving as the length scale of decay rate.

5.2 Dimensional analysis

Dimensional analysis has served as a powerful tool in fluid mechanics for centuries. An important feature of dimensional analysis is to search for the proper variables that can correlate the observed measurements into simplest expressions. That is, to collapse measurements into a single curve if possible. The resulting dimensionless parameters may reveal the physics of the underlying processes. A good example is the analysis of drag coefficient of particles or pressure drop of pipe flows, which leads to the dimensionless Reynolds number, one of the most important dimensionless parameters in boundary layer physics, revealing the balance between inertial and viscous force. For the wind drag on the ocean surface, a key element is that waves moderate the air-sea interface. The representative velocity scale of the wave field is wave phase speed and the length scale is wavelength. If these are chosen to normalize the observations, the measurements can be collapsed into a single cluster of data points. Application of the concept to field data under wind sea conditions indeed improves the representation of the drag coefficient considerably in comparison to C_{10} parameterizations (Fig. 3 and Hwang, 2004, 2005).

On the other hand, the ability to group data in an orderly fashion through judicial choice of scaling factors does not lead automatically to the discovery of the true physics and mechanisms. The coupled air-sea interaction processes are very complicated and the analysis presented above represents a small increment of progress on the parameterization of the drag coefficient of the water surface under fetch limited wave conditions in the field environment (Fig. 3). Counter examples showing a lack of correlation between drag coefficient or dynamic roughness and wave parameters are abundant, especially in laboratory experiments. Ueno and Deushi (2003) present a comprehensive review of many such examples. They perform dimensional analysis of the dynamic roughness parameter assuming wave effects are negligible. The resulting scaling length for z_0 is a function of viscosity (ν), surface tension (τ), and gravity (g). Using the wave-independent scaling, they are able to collapse several laboratory datasets of dynamic roughness measurements (compare their figures 3 and 4). Their scaling equation (21) is applied to the fetch-limited and swell-influenced datasets obtained in the ocean environment assembled by Hwang (2005). The results are displayed in Fig. 8. Because water temperature is not always reported in all datasets, the computation is performed for 5° and 15°C to illustrate the influence of water temperature on the result of the dimensionless parameters. Comparing the dimensionless vs. dimensional representations (left panels vs. right panels), one gets the impression that the wave-independent

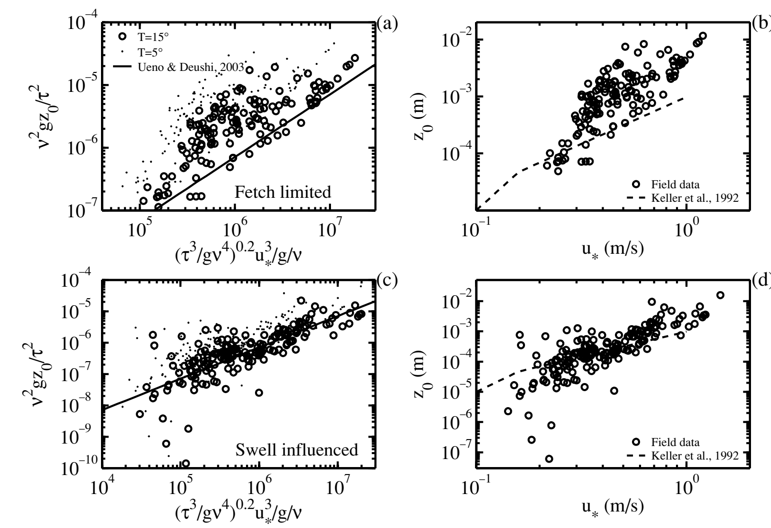

Fig. 8. Application of wave-independent scaling of z_0 (Ueno and Deushi, 2003) to the field data. The top panels (a), (b) are fetch-limited wave conditions, the lower panels (c), (d) are swell-influenced conditions. The dimensionless representations are given on the left panels. The dimensional representations are given on the right panels for comparison.

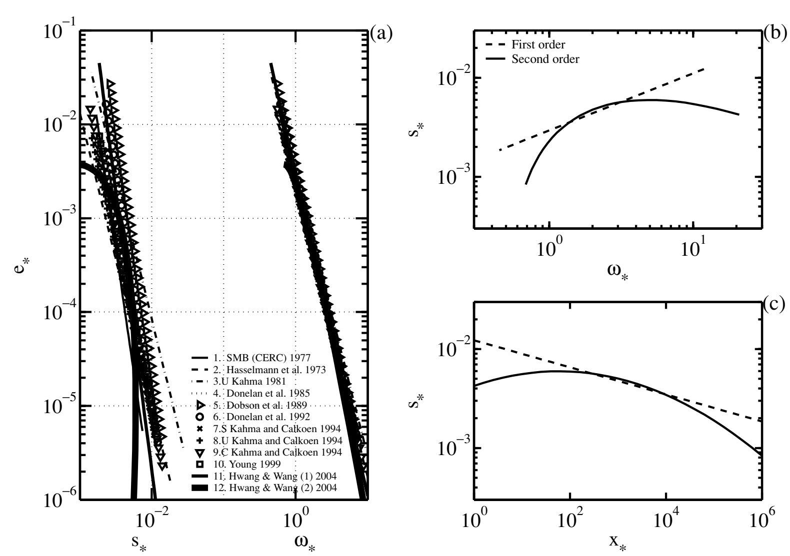

Fig. 9. (a) Fetch-growth similarity laws of wind-generated waves expressed in terms of $e_*(s_*)$ (left-hand set) and $e_*(\omega_*)$ (right-hand set), (b) $s_*(\omega_*)$, and (c) $s_*(x_*)$.

scaling does not really reduce the scatter of data collected from either fetch-limited or swell-influenced wave conditions in the field. Interestingly, while their dimensionless function falls near the lower bound of the fetch-limited measurements (Fig. 8(a)), it runs through the center of the swell-influenced data (Fig. 8(c)). The significance of such "agreement" with mixed sea data is not clear. Indeed, the dimensionally inconsistent empirical expression relating z_0 and u_* given by Keller *et al.* (1992) also compares quite well with the mixed sea data (Fig. 8(d)). The physics involved in the coupled air-sea interaction processes remains challenging and elusive. It is quite possible that among the intertwining factors affecting the wind drag on the water surface, the processes that are important in the laboratory environment may be trivial for the field environment and vise versa. One cannot stress enough the importance of distinguishing the scale differences between laboratory and field, and the need for caution in extending laboratory results to field conditions.

5.3 *Steepness parameter*

Summarizing the comparisons shown in Figs. 4 to 6, it is found that dynamic roughness normalization by rms wave height alone produces as good or even better performance than bi-variable normalization with rms wave height and significant wave steepness. This is somewhat surprising. It is possible that a consistent similarity requires satisfaction of the fetch limited growth condition. When the situation deviates from the fetch limited condition, the influence on steepness is more severe than on the wave frequency or wave variance. Therefore, formulas produced by empirical fitting with imperfect data would yield larger variations on the steepness parameter. An investigation is conducted on 12 different expressions of the fetch limited growth functions reported by Kahma and Calkoen (1992), Young (1999) and Hwang and Wang (2004). It is found that the discrepancies among different fetch limited growth functions amplify significantly when they are expressed in terms of s_*. Figure 9(a) presents the summary result of the investigation, illustrating the consistency of fetch limited growth functions presented in terms of $e_*(\omega_*)$ in comparison with the volatility of the same functions presented in terms of $e_*(s_*)$. In particular, if fetch-dependent growth rate is considered, the significant slope parameter is not a monotonic function of the dimensionless fetch or frequency (Figs. 9(b) and (c)). The sensitive characteristic and nonmonotonic properties of s_* are possibly the main reason that bi-variable normalization using both wave height and steepness parameters is less robust than the single-variable normalizations using rms wave height or wavelength for the dynamic roughness.

6. Summary and Conclusions

Wave-induced dynamic influences on the fluids above and below interfacial waves decay exponentially with distance from the interface. The decay rate is inversely proportional to the wavelength. It is well established in physical oceanography that wavelength serves as the primary length scale for studying the dynamics of wave impacts through the water column. The wave impacts on the fluid above the interface (the atmosphere) are expected to mirror the wave dynamics underwater. It is logical to consider that the vertical elevation in atmospheric measurements influenced by surface waves should scale with the characteristic wavelength of the surface undulations. In this paper, the properties of the drag coefficient and dynamic roughness are investigated for both cases that the vertical scaling length is represented by the surface wavelength and by a fixed distance (10 m height). Results using a fixed scaling length are not expected to collapse data in an orderly manner amenable to interpretation. They can also mislead if dimensionally inconsistent functions are used (e.g., compare Figs. 2(b) and (c)). The influence of wavelength on the magnitude of C_{10} is considerable. This result is substantiated by wind stress data collected under fetch limited conditions (Fig. 3).

Direct wind stress measurements show that the dynamic roughness of the ocean surface represented by a constant Charnock parameter is insufficient and the formulation of the dimensionless roughness needs to include wave properties explicitly. Several different functions have been proposed (9)–(11). As suggested by Donelan (1990), at the present stage, a consistent parameterization of dynamic roughness can only be expected in fetch limited wind-generated wave conditions. Applying the fetch limited growth laws, (9) to (11) are recast into their equivalent forms of $z_{0*}(\omega_*)$ as (22) to (24). Taking into consideration that the rate of wave development varies with wave age, thus that the exponent of the fetch law $e_*(\omega_*)$ varies with ω_*, it is shown that $z_{0*}(\omega_*)$ is expected to have a positive slope for $\omega_* < \sim 2$ and a negative slope for $\omega_* > \sim 2$. Such behavior is evident in the data assembled by Toba *et al*. (1990) and Donelan *et al*. (1993) (Figs. 5 and 6). Finally, the significant slope, s_*, is a very sensitive property of the ocean surface waves. Parameterization of the dynamic roughness including the steepness parameter may limit its range of applicability. Unwanted results may occur when the fitted functions are applied to data outside the parameter range of the original data source.

Acknowledgements

This work is sponsored by the Office of Naval Research (Naval Research Laboratory Program Elements PE61153N and PE62435N). Nancy Mangin assisted in the data digitization and manuscript preparation. (U.S. Naval Research Laboratory Contribution JA/7330-04-0013.)

Appendix A. Fetch Limited Growth Laws

Hwang and Wang (2004) present an analysis of fetch and duration growth functions. The results relevant to the present study are summarized here. Figure A1(a) show the scatter plots of $\omega_*(x_*)$ and $e_*(x_*)$ of the combined data from five field experiments (Burling, 1959; Hasselmann *et al*., 1973; Donelan *et al*., 1985; Dobson *et al*., 1989; Babanin and Soloviev, 1998). The results can be reasonably well represented by simple power-law functions for the fetch range $\sim 10^2 < x_* < \sim 10^4$. For a broader range coverage, the development rate is clearly not a constant. The variable development rate can be obtained from data by using a second order polynomial function in log-log scales. Let

$$Y = \ln y, \text{ and } X = \ln x, \tag{A1}$$

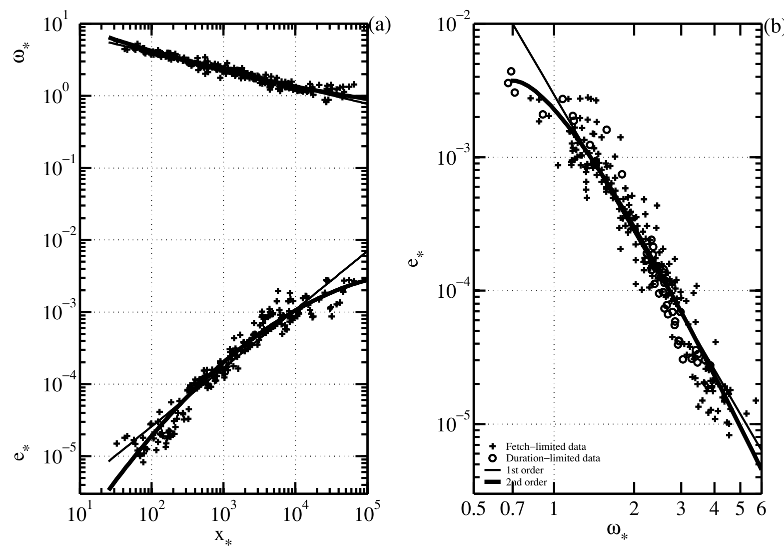

Fig. A1. Fetch limited growth functions in terms of (a) $\omega_*(x_*)$ and $e_*(x_*)$, and (b) $e_*(\omega_*)$. The first and second order fitted curves are also shown (Hwang and Wang, 2004).

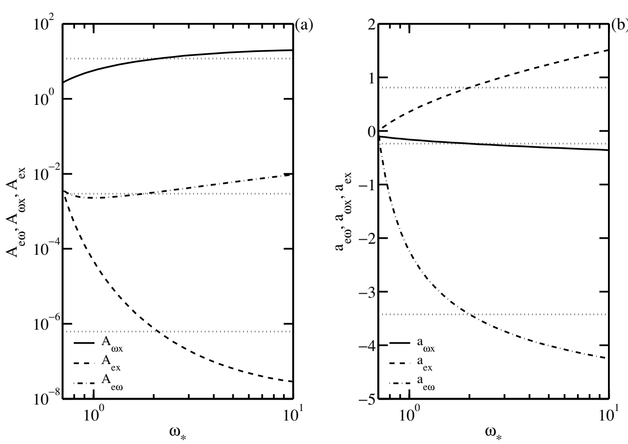

Fig. A2. Local parameters of the fetch limited growth laws, (a) coefficients A_{ex}, $A_{\omega x}$, $A_{e\omega}$, and (b) exponents a_{ex}, $a_{\omega x}$ and $a_{e\omega}$.

where x and y can be either e_*, ω_* or x_*, the polynomial

$$Y = \sum_{n=0}^{N} \alpha_n X^n \tag{A2}$$

is identically

$$y = e^{\alpha_0} x^{\sum_{n=1}^{N} \alpha_n (\ln x)^{n-1}}. \tag{A3}$$

For $N = 1$,

$$y = e^{\alpha_0} x^{\alpha_1} = A_{yx1} x^{a_{yx1}}. \tag{A4}$$

For $N = 2$,

$$y = e^{\alpha_0} x^{\alpha_1 + \alpha_2 \ln x} = A'_{yx2} x^{a'_{yx2}}. \tag{A5}$$

Note that a'_{yx2} is not the local slope of $y(x)$ for $N = 2$. The local slope should be evaluated by

$$a_{yx} = \frac{x}{y}\frac{dy}{dx}, \tag{A6}$$

which yields

$$a_{yx2} = \alpha_1 + 2\alpha_2 \ln x. \tag{A7}$$

The local coefficient A_{yx2} of $y(x) = A_{yx2}\, x^{a_{yx2}}$ can be obtained from (A5) and (A7),

$$A_{yx2} = e^{\alpha_0} x^{-\alpha_2 \ln x}. \tag{A8}$$

The assembled data are used to obtain coefficients A_{yx1}, a_{yx1}, A_{yx2} and a_{yx2} (in terms of α_i) for the functions $e_*(x_*)$, $\omega_*(x_*)$ and $e_*(\omega_*)$. The data and fitted curves are shown in Fig. A1 and the fitting coefficients are listed in Table A1. Figure A2 plots A_{yx2} and a_{yx2} for the functions $e_*(x_*)$, $\omega_*(x_*)$ and $e_*(\omega_*)$.

For the purpose of presenting the coefficient A and exponent a in terms of ω_* using the fitting coefficients

Table A1. Polynomial fitting coefficients for data presented in Fig. A1.

	First order		Second order		
	α_0	α_1	α_0	α_1	α_2
$\omega_*(x_*)$	2.4732	−0.2368	3.0377	−0.3990	0.0110
$e_*(x_*)$	−14.2950	0.8106	−17.6158	1.7645	−0.0647
$e_*(\omega_*)^\#$	−5.8936	−3.3341	−6.1384	−2.4019	−0.6102

#Note the coefficients for $e_*(\omega_*)$ from least-square fitting as tabulated here are slightly different from those computed from the coefficients of $e_*(x_*)$ and $\omega_*(x_*)$ (Hwang and Wang, 2004), the latter are used in Fig. A2.

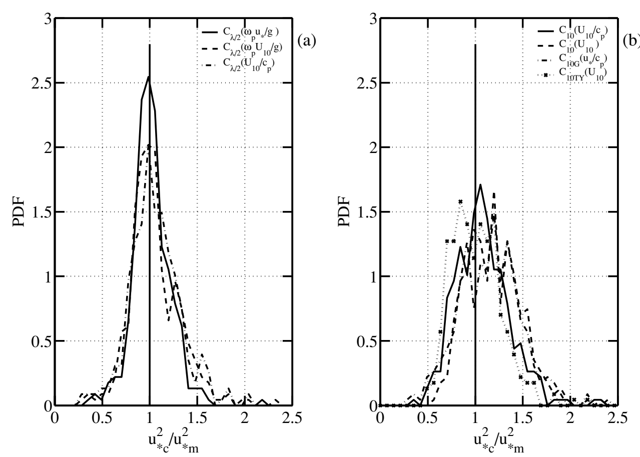

Fig. B1. Probability density distribution of the ratio of computed and measured wind stress, $R = u^2_{*c}/u^2_{*m}$, obtained by different expressions of the drag coefficient. (a) $C_{\lambda/2}$ parameterizations, (b) C_{10} parameterizations (Hwang, 2005).

for $e_*(x_*)$ and $\omega_*(x_*)$, it is necessary to develop an expression of $x_*(\omega_*)$. Expressing

$$\omega_* = e^{b_0} x_*^{b_1 + b_2 \ln x_*}, \tag{A9}$$

which is a quadratic equation of $\ln\omega_*$ in terms of $\ln x_*$, x_* can be written as

$$x_* = \exp\left\{\frac{-b_1 - \sqrt{b_1^2 - 4b_2(b_0 - \ln\omega_*)}}{2b_2}\right\}. \tag{A10}$$

Appendix B. Practical Issues of Wavelength Scaling

The practical aspect of the wavelength scaling for the drag coefficient and dynamic roughness of the ocean surface is addressed by Hwang (2005). A brief summary is presented here. As shown in Fig. 3(a), the drag coefficient referenced to $U_{\lambda/2}$ can be expressed as a simple function of $\omega_p u_*/g$ (26). For many practical applications u_* is not available. A different parameterization function of $C_{\lambda/2}$ based on U_{10} and suitable wave parameters needs to be developed. Empirically, from experimenting with different dimensionless parameters, it is found that $C_{\lambda/2}(\omega_p U_{10}/g)$ or $C_{\lambda/2}(U_{10}/c_p)$ represents a fair alternative to $C_{\lambda/2}(\omega_p u_*/g)$. The fitting coefficients and statistics of the correlation coefficient and rms difference for six different parameterization schemes examined by Hwang (2005) are summarized in the following equation

$$C_{\lambda/2} = \begin{cases}
1.289\times10^{-3}\left(\dfrac{\omega_p U_{10}}{g}\right)^{0.815}, \quad Q = 0.89, \; S = 0.024, & \text{(B1a)}\\[2ex]
1.145\times10^{-3}\left(\dfrac{U_{10}}{c_p}\right)^{0.825}, \quad Q = 0.89, \; S = 0.025, & \text{(B1b)}\\[2ex]
1.163\times10^{-3}\left(\dfrac{\omega_p U_{\lambda/2}}{g}\right)^{0.989}, \quad Q = 0.88, \; S = 0.025, & \text{(B1c)}\\[2ex]
1.039\times10^{-3}\left(\dfrac{U_{\lambda/2}}{c_p}\right)^{0.947}, \quad Q = 0.85, \; S = 0.028, & \text{(B1d)}\\[2ex]
1.220\times10^{-2}\left(\dfrac{\omega_p u_*}{g}\right)^{0.704}, \quad Q = 0.95, \; S = 0.017, & \text{(B1e)}\\[2ex]
1.086\times10^{-2}\left(\dfrac{u_*}{c_p}\right)^{0.696}, \quad Q = 0.94, \; S = 0.019. & \text{(B1f)}
\end{cases}$$

A comparison is carried out to quantify the difference in wind stress computation using several different parameterization functions of the drag coefficient in terms of $C_{\lambda/2}$ and C_{10}. The datasets used in that comparison study include fetch-limited wind seas and swell-influenced mixed seas. Detailed tabulated statistics and graphs of comparison for different expressions of the drag coefficient are provided. An example of the comparison is shown in Fig. B1, illustrating convincingly that wind stress computed with $C_{\lambda/2}$ functions is more accurate than that computed with C_{10} functions. At this stage, the wave information in addition to U_{10} input is needed. In future development, the fetch- or duration-limited growth laws may be used to further reduce the number of external parameters required for wind-sea dominant conditions. This paper represents an effort toward achieving that goal. With swell influence, it is expected that the relation will be considerably more complicated. It is therefore quite critical to have a firm grasp of the baseline case of wind-sea dominant conditions. The development so far shows the advantage of $C_{\lambda/2}$ over C_{10} for representing the drag coefficient of the ocean surface under windsea dominated conditions.

References

Anctil, F. and M. A. Donelan (1996): Air-water momentum flux observed over shoaling waves. *J. Phys. Oceanogr.*, **26**, 1344–1353.

Babanin, A. V. and Y. P. Soloviev (1998): Field investigation of transformation of the wind wave frequency spectrum with fetch and the stage of development. *J. Phys. Oceanogr.*, **28**, 563–576.

Banner, M. L. and W. K. Melville (1976): On the separation of air flow over water waves. *J. Fluid Mech.*, **77**, 825–842.

Burling, R. W. (1959): The spectrum of waves at short fetches. *Dtsch. Hydrogr. Z.*, **12**, 96–117.

Charnock, H. (1955): Wind stress on a water surface. *Quart. J. Roy. Meteorol. Soc.*, **81**, 639.

Dobson, F., W. Perrie and B. Toulany (1989): On the deep-water fetch laws for wind-generated surface gravity waves. *Atmos.-Ocean*, **27**, 210–236.

Donelan, M. A. (1979): On the fraction of wind momentum retained by waves. p. 141–159. In *Marine Forecasting*, ed. by J. C. J. Nihoul, Elsevier.

Donelan, M. A. (1990): Air-sea interaction. p. 239–292. In *The Sea—Volume 9: Ocean Engineering Science*, ed. by B. LeMehaute and D. M. Hanes, Wiley Interscience.

Donelan, M. A., J. Hamilton and W. H. Hui (1985): Directional spectra of wind-generated waves. *Phil. Trans. Roy. Soc. Lond.*, **A315**, 509–562.

Donelan, M. A., F. W. Dobson, S. D. Smith and R. J. Anderson (1993): On the dependence of sea surface roughness on wave development. *J. Phys. Oceanogr.*, **23**, 2143–2149.

Hasselmann, K. *et al.* (1973): Measurements of wind-wave growth and swell decay during the Joint North Sea Wave Project (JONSWAP). *Dtsch. Hydrogr. Z.*, Suppl. A, 8, **12**, 95 pp.

Hwang, P. A. (2004): Influence of wavelength on the parameterization of drag coefficient and surface roughness. *J. Oceanogr.*, **60**, 835–841.

Hwang, P. A. (2005): Comparison of the ocean surface wind stress computed with different parameterization functions of the drag coefficient. *J. Oceanogr.*, **61**, 91–107.

Hwang, P. A. and D. W. Wang (2004): Field measurements of duration limited growth of wind-generated ocean surface waves at young stage of development. *J. Phys. Oceanogr.*, **34**, 2316–2326. (Corrigendum, **35**, 268–270, 2005.)

Janssen, J. A. M. (1997): Does wind stress depend on sea-state or not?—A statistical error analysis of HEXMAX data. *Bound.-Layer Meteorol.*, **83**, 479–503.

Jones, I. S. F. and Y. Toba (eds.) (2001): *Wind Stress over the Ocean*. Cambridge Univ. Press, 307 pp.

Kahma, K. K. and C. J. Calkoen (1992): Reconciling discrepancies in the observed growth of wind-generated waves. *J. Phys. Oceanogr.*, **22**, 1389–1405.

Kawai, S. (1982): Structure of air flow separation over wind wave crests. *Bound.-Layer Meteorol.*, **23**, 503–521.

Kawai, S., K. Okada and Y. Toba (1977): Support of the 3/2-power law and the $gu_*\sigma^{-4}$-spectral form for growing wind waves with field observation data. *J. Oceanogr. Soc. Japan*, **33**, 137–150.

Keller, M. R., W. C. Keller and W. J. Plant (1992): A wave tank study of the dependence of X band cross sections on wind speed and water temperature. *J. Geophys. Res.*, **97**, 5771–5792.

Kitaigorodskii, S. A. (1973): *The Physics of Air-Sea Interaction*. Israel Program for Scientific Translations, Jerusalem (English translation), 237 pp.

Kitaigorodskii, S. A. and Y. A. Volkov (1965): On the roughness parameter of the sea surface and the calculation of momentum flux in the near surface layer of the atmosphere. *Izv., Atmos. Oceanic Phys.*, **1**, 973–988.

Makin, V. K. (2003): A note on a parameterization of the sea drag. *Bound.-Layer Meteorol.*, **106**, 593–600.

Makin, V. K. and V. N. Kudryavtsev (1999): Coupled sea surface-atmosphere model. 1. Wind over waves coupling. *J. Geophys. Res.*, **104**, 7613–7623.

Makin, V. K. and V. N. Kudryavtsev (2002): Impact of dominant waves on sea drag. *Bound.-Layer Meteorol.*, **103**, 83–99.

Merzi, N. and W. H. Graf (1985): Evaluation of the drag coefficient considering the effects of mobility of the roughness elements. *Ann. Geophys.*, **3**, 473–478.

Miles, J. W. (1957): On the generation of surface waves by shear flow. *J. Fluid Mech.*, **3**, 185–204.

Oost, W. A., G. J. Komen, C. M. J. Jacobs and C. Van Oort (2002): New evidence for a relation between wind stress and wave age from measurements during ASGAMAGE. *Bound.-Layer Meteorol.*, **103**, 409–438.

Phillips, O. M. (1977): *The Dynamics of the Upper Ocean*. Cambridge Univ. Press, Cambridge, U.K., 336 pp.

Schlichting, H. (1968): *Boundary-Layer Theory*, translated by J. Kestin. McGraw-Hill Book Co., New York, 748 pp.

Smith, S. D., R. J. Anderson, W. A. Oost, C. Kraan, N. Maat, J. DeCosmo, K. B. Katsaros, K. L. Davidson, K. Bumke, L. Hasse and H. M. Chadwick (1992): Sea surface wind stress

and drag coefficients: The HEXOS results. *Bound.-Layer Meteorol.*, **60**, 109–142.
Stewart, R. W. (1974): The air-sea momentum exchange. *Bound.-Layer Meteorol.*, **6**, 151–167.
Taylor, P. K. and M. J. Yelland (2001): The dependence of sea surface roughness on the height and steepness of the waves. *J. Phys. Oceanogr.*, **31**, 572–590.
Toba, Y., N. Iida, H. Kawamura, N. Ebuchi and I. S. F. Jones (1990): Wave dependence of sea-surface wind stress. *J. Phys. Oceanogr.*, **20**, 705–721.
Ueno, K. and M. Deushi (2003): A new empirical formula for the aerodynamic roughness of water surface waves. *J. Oceanogr.*, **59**, 819–831.
Volkov, Y. (2001): The dependence on wave age. p. 206–217. In *Wind Stress over the Ocean*, ed. by I. S. F. Jones and Y. Toba, Cambridge Univ. Press, New York.
Young, I. R. (1999): *Wind Generated Ocean Waves*. Elsevier, Amsterdam, the Netherlands, 288 pp.